ACS Energy LETTERS

http://pubs.acs.org/journal/aelccp

LETTER

Recombination in Perovskite Solar Cells: Significance of Grain Boundaries, Interface Traps, and Defect Ions

Tejas S. Sherkar,[†] Cristina Momblona,[‡] Lidón Gil-Escrig,[‡] Jorge Ávila,[‡] Michele Sessolo,[‡] Henk J. Bolink,[‡] and L. Jan Anton Koster*[,†]

[†]Zernike Institute for Advanced Materials, University of Groningen, Nijenborgh 4, 9747AG Groningen, The Netherlands
[‡]Instituto de Ciencia Molecular, Universidad de Valencia, C/Catedrático J. Beltrán 2, 46980 Paterna Valencia, Spain

Supporting Information

ABSTRACT: Trap-assisted recombination, despite being lower as compared with traditional inorganic solar cells, is still the dominant recombination mechanism in perovskite solar cells (PSCs) and limits their efficiency. We investigate the attributes of the primary trap-assisted recombination channels (grain boundaries and interfaces) and their correlation to defect ions in PSCs. We achieve this by using a validated device model to fit the simulations to the experimental data of efficient vacuum-deposited p−i−n and n−i−p $CH_3NH_3PbI_3$ solar cells, including the light intensity dependence of the open-circuit voltage and fill factor. We find that, despite the presence of traps at interfaces and grain boundaries (GBs), their neutral (when filled with photogenerated charges) disposition along with the long-lived nature of holes leads to the high performance of PSCs. The sign of the traps (when filled) is of little importance in efficient solar cells with compact morphologies (fused GBs, low trap density). On the other hand, solar cells with noncompact morphologies (open GBs, high trap density) are sensitive to the sign of the traps and hence to the cell preparation methods. Even in the presence of traps at GBs, trap-assisted recombination at interfaces (between the transport layers and the perovskite) is the dominant loss mechanism. We find a direct correlation between the density of traps, the density of mobile ionic defects, and the degree of hysteresis observed in the current−voltage (J−V) characteristics. The presence of defect states or mobile ions not only limits the device performance but also plays a role in the J−V hysteresis.

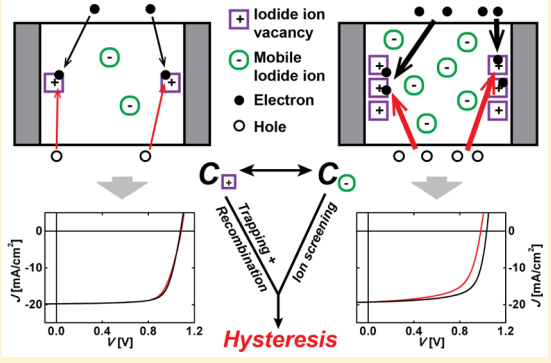

Thin-film solar cells making use of hybrid halide perovskites, $CH_3NH_3PbX_3$ (X = Cl, Br, I), as a photoactive material show device power conversion efficiencies upward of 22%.[1] High device efficiency arises from the many desirable properties of perovskites, including a high absorption coefficient, high carrier mobilities, and long charge carrier diffusion lengths.[2−4] Efficient perovskite solar cells (PSCs) can be prepared by vacuum deposition[5,6] and solution processing[7,8] and in p−i−n as well as n−i−p configurations.[9] While the efficiency of PSCs is high, it is still far from the theoretical maximum (31%).[10] One of the reasons (others being optical losses, nonideal transport layers, and contact energy offsets) is the recombination of charge carriers in the device, which reduces the fill factor (FF) and the open-circuit voltage (V_{OC}) of the solar cell. At solar fluences, radiative recombination (between free electrons and free holes) is weak in PSCs.[11] On the other hand, nonradiative recombination has been shown to be the dominant recombination mechanism in PSCs,[12,13] which limits the efficiency of existing PSCs.[14,15]

Nonradiative recombination takes place when a electron (or hole) trapped in a defect/impurity (energy level in the band gap of the perovskite) recombines with a hole (or electron) in the valence (or conduction) band of the perovskite. In polycrystalline perovskite thin films, defects or impurities are likely to be concentrated at grain boundaries (GBs) and at film surfaces.[16−18] The surface of the photoactive perovskite in PSCs is covered with ETL and HTL, which forms an interface. While nonradiative recombination at interfaces has been shown to severely influence the PSC performance,[15] the role of the GBs on the overall device performance is still under debate.[19−22] A few studies suggest that traps at GBs lead to increased trap-assisted recombination,[23,24] insulating products (e.g., PbI_2) formed at GBs passivate the traps and hence minimize trap-assisted recombination,[19,20] and GBs act as hole

Received: March 16, 2017
Accepted: May 2, 2017
Published: May 2, 2017

DOI: 10.1021/acsenergylett.7b00236
ACS Energy Lett. 2017, 2, 1214−1222

transport highways, which leads to improved hole collection.[21] With the nature of GBs possibly changing with processing conditions and stoichiometry,[22,25] it is important to investigate their role on the charge carrier dynamics in PSCs and quantify their influence (detrimental or otherwise) on the device performance. This would help to identify appropriate approaches for further increasing the efficiency of PSCs.

GBs are ubiquitous in polycrystalline films and are formed due to a break in the crystal structure of the material. The different orientations of neighboring crystal grains give rise to dislocations, misplaced atoms (interstitials), vacancies, distorted bond angles, and bond distances at the GBs.[26] These GBs are known to play a critical role in the charge carrier dynamics and photophysics of CdTe, poly-Si, and copper indium gallium selenide (CIGS) thin films used in solar cells.[27−30] Several GB models exist in the literature to explain their influence on the charge carrier dynamics in inorganic polycrystalline solar cells.[31−33] However, hybrid perovskites are different from the above-mentioned inorganic photovoltaic materials in terms of doping levels and the nature of GB defect traps. Perovskites are lightly doped materials, and due to the presence of charged ionic defects, it is likely that the traps are electrically charged when empty[34−36] and neutral when filled with photogenerated charges. A different perspective to GB physics is thus essential in the case of PSCs. It could help answer the question, is there a need to move toward single-crystalline materials or are polycrystalline films prepared using existing methods sufficient to achieve high-performing PSCs?

In this Letter, we investigate the attributes of the primary trap-assisted recombination channels, namely, GBs and interfaces, and their correlation to ionic defects in existing PSCs. We accomplish this by using our device model[15] to fit the simulation to the experimental data of vacuum-deposited p−i−n and n−i−p $CH_3NH_3PbI_3$ solar cells.[9] The model takes as input the full experimental data sets, and the only free parameters (to fit) are the carrier mobility in the perovskite and the trap density plus the charge capture coefficients. The model achieves excellent agreement with the experimental measurements (for both p−i−n and n−i−p cells), including the light intensity dependence of the V_{OC} and FF. We find that we can quantitatively describe all of the experimental data set only when we consider trap-assisted recombination at GBs and predominantly at interfaces (HTL/perovskite and perovskite/ETL) and weak bimolecular recombination in the perovskite absorber, ruling out the scenario of strong bulk trap-assisted recombination in the perovskite. Despite the presence of traps, their neutral (when filled) disposition along with the long-lived nature of holes leads to the high performance of PSCs. The sign (if charged or neutral when filled) of traps is of little importance in efficient solar cells with compact morphologies (fused GBs, low trap density). On the other hand, solar cells that have noncompact morphologies (open GBs, high trap density) are sensitive to the sign of the traps and hence to the preparation methods (e.g., under/overstoichiometric routes, environmental conditions). Even in the presence of traps at GBs, trap-assisted recombination at interfaces is the dominant recombination channel. Finally, we simulate fast forward/reverse current−voltage (J−V) scans, which reveal little J−V hysteresis, consistent with that observed experimentally for the p−i−n cell.[9] We observe direct correlation between the density of traps, the density of mobile ionic defects, and the degree of hysteresis in PSCs. Defect states (or mobile ions) not only retard the device performance but also play a role in the J−V hysteresis. Finally, we give an estimate of the mobile ion density in this specific set of solar cells studied here.

The experimental data considered in this Letter were obtained from full vacuum-deposited $CH_3NH_3PbI_3$ devices prepared by some of the authors and published recently.[9] Both p−i−n and n−i−p device configurations are studied (Figure 1),

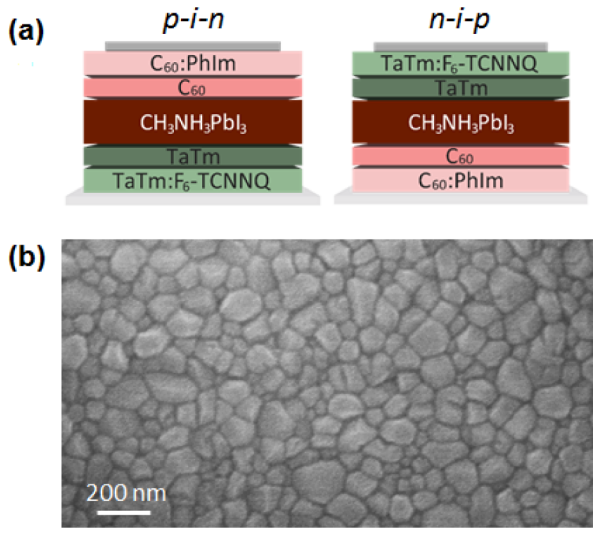

Figure 1. (a) Schematics of the vacuum-deposited perovskite cells used and (b) scanning electron microscope (SEM) image of the $CH_3NH_3PbI_3$ surface.

where i is the perovskite absorber layer, p is the hole transport layer (HTL), and n is the electron transport layer (ETL). For the p−i−n cell, indium tin oxide (ITO) and silver (Ag) are used as the anode and cathode, respectively, and for the n−i−p cell, the anode is gold (Au) and the cathode is ITO. The HTL is composed of a 10 nm thick film of *N*4,*N*4,*N*4″,*N*4″-tetra([1,1′-biphenyl]-4-yl)-[1,1′:4′,1″-terphenyl]-4,4″-diamine (TaTm) in contact with the perovskite, followed by a 40 nm thick TaTm film doped with 2,2′-(perfluoronaphthalene-2,6-diylidene) dimalononitrile (F_6-TCNNQ) in contact with the anode. Analogously, the ETL comprises an undoped C_{60} fullerene film (10 nm) and a C_{60} layer (40 nm) doped with *N*1,*N*4-bis(tri-*p*-tolylphosphoranylidene)-benzene-1,4-diamine (PhIm) in contact with the cathode. The perovskite ($CH_3NH_3PbI_3$) thin films are prepared by co-evaporation of CH_3NH_3I and PbI_2 in a vacuum chamber, to a final thickness of 500 nm. The perovskite shows a band-to-band transition at 780 nm, which translates into a band gap (E_{gap}) of 1.59 eV.[9] The p−i−n and n−i−p solar cells show efficiencies of around 16 and 18%, respectively, with a record efficiency of 20.3% using the n−i−p configuration.[9] Doping of HTL and ETL increases their conductivity and also increases the electric field strength in the perovskite layer, resulting in efficient charge extraction from the perovskite to the external contacts.[9,15] This is reflected in a high FF and V_{OC} for both p−i−n and n−i−p cells.[9]

We recently developed a device model[15] that describes the operation of PSCs and quantitatively explains the role of contacts, the ETL and HTL, charge generation, transport of charge carriers, and recombination. Our 1D device model is based on the drift−diffusion equations for electrons and holes throughout the device and on solving the Poisson equation in one dimension. In the perovskite layer, the absorption of light generates free electrons and holes. The transport of these free

DOI: 10.1021/acsenergylett.7b00236
ACS Energy Lett. 2017, 2, 1214−1222

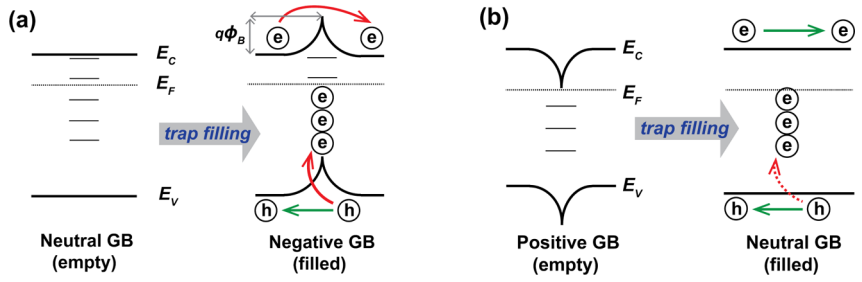

Figure 2. (a) In typical inorganic solar cells (poly-Si, CdTe), the empty neutral traps at GBs and interfaces when filled with electrons result in a weakened transport due to the potential barrier ($q\phi_B$) and the nonradiative recombination between holes and trapped electrons is strong. (b) In PSCs, it is likely that the empty traps are positively charged due to accumulated iodide vacancies (V_I^+) at GBs and interfaces. Therefore, when filled with electrons, the traps are neutral, electron transport is relatively unaffected, and nonradiative recombination is weak.

charges is governed by drift−diffusion and electrically induced drift; for electrons[37]

$$J_n = -qn\mu_n\frac{\partial V}{\partial x} + qD_n\frac{\partial n}{\partial x} \tag{1}$$

and for holes

$$J_p = -qp\mu_p\frac{\partial V}{\partial x} - qD_p\frac{\partial p}{\partial x} \tag{2}$$

where J_n and J_p are electron and hole current densities, respectively, q is the electronic charge (1.602×10^{-19} C), V is the electrostatic potential, n and p are electron and hole concentrations, μ_n and μ_p are electron and hole mobilities, and D_n and D_p are electron and hole diffusion constants, respectively. The diffusion constants are assumed to obey the Einstein relation.[37]

The defect ion current density (J_a, anion; J_c, cation) is also given by the equations above. However, because the electrodes are ion-blocking, $J_a = J_c = 0$.

The electric potential throughout the device is solved from the Poisson equation

$$\frac{\partial}{\partial x}\left(\epsilon\frac{\partial V}{\partial x}\right) = -q(p - n + N_D^+ - N_A^- + X_c - X_a + Q_T\Sigma_T f_T) \tag{3}$$

where ϵ is the permittivity, N_A^- and N_D^+ are the ionized p-type and n-type doping, respectively, and X_c and X_a are the cationic and anionic defect densities,[36,38−40] respectively, in the perovskite absorber. The trap density is Σ_T, the sign of the trap when filled is $Q_T \in \{-1, 0, 1\}$, and the occupation probability of the trap is $f_{T,\nu=n,p}$, which is given by

$$f_{T,\nu=n,p} = \left[1 + \left(\frac{g_{0,\nu}}{g_{1,\nu}}\right)\left(\frac{\nu}{N_{cv}}\exp(E_{trap}/V_t)\right)^{\alpha}\right]^{-1} \tag{4}$$

where $g_{0,1}$ are the degeneracy factors of empty and filled trap levels, respectively, N_{cv} is the effective density of states of both the conduction and valence band, E_{trap} ($=E_{gap}/2$) is the midgap trap energy level, α is the sign of the trapped charge carrier (1 for holes, −1 for electrons), and $V_t = kT/q$ is the thermal voltage, with k being the Boltzmann constant and T the temperature. We neglect the degeneracy of traps and set $g_0/g_1 = 1$.

The boundary condition on the electrostatic potential is

$$q(V(L) - V(0) + V_{app}) = W_c - W_a \tag{5}$$

with V_{app} being the externally applied voltage and W_a and W_c the anode and cathode work functions, respectively. The built-in potential is then given by $V_{bi} = (W_c - W_a)/q$.

The boundary conditions for charge carrier densities at electrode contacts are given by[15]

$$n, p = N_{cv}\exp(-\phi_{n,p}/V_t) \tag{6}$$

where $\phi_{n,p}$ is the offset (in eV) between the cathode (anode) work function and the conduction (valence) band of the perovskite.

The generated charge carriers in $CH_3NH_3PbI_3$ can recombine via both bimolecular and trap-assisted mechanisms. The bimolecular recombination rate (R_{BR}) is given by

$$R_{BR} = k_{BR}(np - n_i^2) \tag{7}$$

where k_{BR} is the bimolecular recombination constant and n_i is the intrinsic carrier concentration. The trap-assisted recombination rate (R_{SRH}) is given by the Shockley−Read−Hall (SRH) equation[37]

$$R_{SRH} = \frac{C_nC_p\Sigma_T}{C_n(n + n_1) + C_p(p + p_1)}(np - n_i^2) \tag{8}$$

where C_n and C_p are the capture coefficients for electrons and holes, respectively. C_n denotes the probability per unit time that the electron in the conduction band will be captured for the case that the trap is filled with a hole and able to capture the electron. Correspondingly, C_p denotes the probability per unit time that the hole in the valence band will be captured when the trap is filled with a electron and able to capture the hole. The constants n_1 and p_1 are defined as

$$n_1 = n(f_{T,n}^{-1} - 1) \qquad p_1 = p(f_{T,p}^{-1} - 1)^{-1} \tag{9}$$

The interface traps are located in a 2 nm thick region at HTL/perovskite ($\Sigma_{T,p}$) and perovskite/ETL ($\Sigma_{T,n}$) material interfaces and operate as recombination centers.[15] Recombination is most effective when traps are located midgap, and it is shown that recombination dynamics for an arbitrary distribution of traps near the middle of the band gap is identical.[41]

The details of the slow ("stabilized") J−V scans used to fit to the experimental data, fast forward/reverse J−V scans, and hysteresis simulations, which include preconditioning, are presented in the Supporting Information (SI).

The numerical approaches and procedures to solve the above-mentioned equations can be found in refs 15 and 42.

Defects and impurities located at GBs and surfaces can act as traps for photogenerated charge carriers. In hybrid PSCs,

DOI: 10.1021/acsenergylett.7b00236
ACS Energy Lett. 2017, 2, 1214−1222

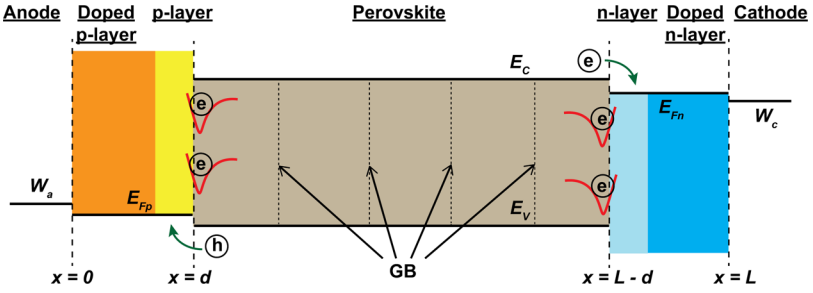

Figure 3. The p−i−n device skeleton showing the energy levels, interface traps (red), and GBs (dashed lines). Upon illumination, free electrons and holes are transported through the respective materials and are extracted at the electrodes.

electrons are the trapped carriers.[12,43,44] A negative GB is formed when electrons fill the empty uncharged GB traps, and a neutral GB is formed when electrons fill the empty charged traps. Figure 2 shows the case of a filled negative and a filled neutral GB. It is clear that GBs can act as (1) potential barriers ($E_B = q\phi_B$) for electrons, which impedes their transport from one crystallite to another and thus affects their long-range mobility, and (2) recombination centers where the trapped electrons recombine nonradiatively with free holes in the valence band. Because hybrid perovskites are ionic conductors, the associated traps are expected to be electrically charged.[34−36]

Positively charged iodide vacancies (V_I^+) are the dominant defect ions, as indicated by recent theoretical studies.[35,38] Migration of these defect ions has been shown to occur via the GBs rather than the crystal bulk.[16] GBs typically show weak emission in photoluminescence (PL) measurements,[23,45] suggesting trapping and nonradiative recombination of carriers. It is therefore likely that accumulation of V_I^+ at GBs and surfaces (or interfaces) induces trap states that act as recombination centers for photogenerated carriers. Few theoretical studies predict the iodide vacancies to have energy states outside of the band gap;[46] however, these calculations are performed considering iodide vacancies as bulk point defects. The more relevant and performance-limiting features are the GBs and interfaces (or surfaces) where iodide vacancies and ions are most likely to reside at in thin films.[16,20] Many recent experimental results point to the trapping nature of the accumulated iodide vacancies at GBs and interfaces.[43,45,47] A recently published theoretical study looked at carrier trapping at surface defects and reported that iodide vacancies do exhibit energy states inside of the band gap.[48] Therefore, we assume that the GB traps (accumulated V_I^+) when filled with charge carriers (electrons) are likely to be electrically neutral. Filled neutral traps are less likely to lead to rapid recombination as compared to filled charged traps, confirming the light-soaking experiments in PSCs where trap filling by photogenerated charges reduces the trap-assisted recombination in the device.[47]

A refinement of our full 3D drift−diffusion simulation[49] is currently a work in progress to take into account the accumulation of ionic defects at 3D GBs to explain the recently reported anomalous photovoltaic effect.[50]

In our devices, the experimentally observed crystal size is ∼100 nm on average.[9] Therefore, we incorporate GBs in our device model and place them L_{GB} = 100 nm apart along the thickness of the perovskite absorber. The traps at GBs ($\Sigma_{T,GB}$) and at interfaces ($\Sigma_{T,p}$, $\Sigma_{T,n}$) are charged when empty and neutral when filled. Because the device is electrically neutral in the dark, we assume in the model that the charged empty traps (accumulated V_I^+) are compensated by an equal density (volume) of mobile iodide ions given by

$$X_a = (n_{GB} \times \Sigma_{T,GB} + \Sigma_{T,n} + \Sigma_{T,p})/L_{abs} \quad (10)$$

where n_{GB} is the number of GBs along the absorber thickness (L_{abs}). This makes the perovskite slightly p-type, in agreement with the literature.[43,44,51] The distribution of these mobile iodide ions in the perovskite layer is solved from the coupled continuity and Poisson equation discussed before and according to the device operating conditions (i.e., external bias, illumination, preconditioning), as detailed in SI.

Now, we fit the simulations to the experimental data of both p−i−n and n−i−p solar cells prepared by vacuum deposition.[9] The p−i−n device skeleton is shown in Figure 3. In the n−i−p device, the p and n layers are interchanged by reversing the order of vacuum deposition of the same materials.[9] The only difference is the top metal contact, silver (Ag) for the p−i−n cell and gold (Au) for the n−i−p cell. The model takes as input an extensive experimental data set (Table 1), and the only free parameters (to fit) are the carrier mobility in the perovskite and the trap density plus the charge capture coefficients.

We find that the model achieves quantitative agreement with the experimental data sets (both p−i−n and n−i−p cell) only when we consider (i) trap-assisted recombination at interfaces (HTL/perovskite and perovskite/ETL), (ii) trap-assisted recombination at GBs, and (ii) weak bimolecular recombination in the perovskite layer. When we considered other scenarios, mainly of bulk trap-assisted recombination in the perovskite, the simulations did not fit the experimental data of the light intensity dependence of the V_{OC} and FF. The FF is more sensitive to the location and strength of different recombination channels in the device. For example, if we consider bulk trap-assisted recombination in simulations, the FF shows a positive dependence on light intensity. However, in our devices, we see the FF initially increasing and then decreasing with lowering of light intensity. Therefore, we rule out bulk trap-assisted recombination in perovskite as a primary recombination channel and a (device) performance-limiting attribute.

The experimental data under "stabilized" conditions (slow scan) for both p−i−n and n−i−p cells are shown in Figure 4a. The devices are illuminated by a standard AM 1.5G light source. Figure 4a also shows the fit to the experimental $J-V$ characteristics of both cells. The simulated fit is also performed under "stabilized" conditions, that is, an infinitely slow $J-V$ scan, where all mobile ions (calculated from eq 10) are redistributed in the perovskite layer according to the steady-state operating condition (applied bias, illumination) during the scan. In order to fit the simulation to the experimental data, we find that we need weak bimolecular recombination in the perovskite bulk and trap-assisted recombination at interfaces (HTL/perovskite and perovskite/ETL) and at GBs. The

DOI: 10.1021/acsenergylett.7b00236
ACS Energy Lett. 2017, 2, 1214−1222

Table 1. Parameters Used in the Device Simulation of Both p−i−n and n−i−p Solar Cells to Simultaneously Fit to the *J*−*V* Curves and Light Intensity Dependence of V_{OC} and FF

parameter	symbol	value	
perovskite band gap	E_{gap}	1.59 eV	ref 9
density of states (DOS)	N_{cv}	3.1×10^{18} cm^{-3}	
perovskite conduction band minimum	E_c	−5.43 eV	ref 9
perovskite valence band maximum	E_v	−3.84 eV	ref 9
TaTm HOMO level	E_{HOMO}	−5.4 eV	ref 9
C60 LUMO level	E_{LUMO}	−4.0 eV	ref 53
built-in voltage	V_{bi}	1.4 V	ref 9
hole mobility in TaTm (HTL)	$\bar{\mu}_p$	4×10^{-3} cm^2/(V s)	
electron mobility in C60 (ETL)	$\bar{\mu}_n$	3×10^{-2} cm^2/(V s)	ref 53
perovskite relative permittivity	ϵ	24.1	ref 54
TaTm relative permittivity	ϵ_p	3	
C60 relative permittivity	ϵ_n	3.9	ref 55
ionized doping in C60/PhIm	N_D^+	5×10^{18} cm^{-3}	ref 9
ionized doping in TaTm/F_6TCNNQ	N_A^-	1×10^{16} cm^{-3}	ref 9
bimolecular recombination constant	k_{BR}	1×10^{-9} cm^3 s^{-1}	ref 11
electron and hole mobility in perovskite	μ_n,μ_p	5 cm^2/(V s)	fit
HTL/perovskite interface trap density	$\Sigma_{T,p}$	1×10^{10} cm^{-2}	fit
perovskite/ETL interface trap density	$\Sigma_{T,n}$	2×10^{9} cm^{-2}	fit
GB trap density	$\Sigma_{T,GB}$	1.8×10^{9} cm^{-2}	fit
electron and hole capture coefficients	C_n, C_p	1×10^{-6}, 1×10^{-8} cm^3 s^{-1}	fit
number of grid points		1000	
grid spacing	Δx	0.6 nm	
maximum charge generation rate	G_{max}	5.4×10^{21} cm^{-3} s^{-1}	

simulation of p−i−n and n−i−p cells is performed using the same set of device parameters, including all of the fitting parameters. The only change is the removal of the hole energetic offset (0.1 eV) in n−i−p cells where gold is used as the anode as compared to ITO as the anode in the p−i−n cell, which has a lower work function than gold (Au).[9] The calculated charge generation profile in both cells is shown in Figure 4b. The material optical constants (η, κ) as input to the transfer matrix model[52] in order to calculate the generation profile in p−i−n and n−i−p cells are obtained from the literature and are provided in the SI. Table 1 lists all of the device parameters used in the simulation to fit to the experimental data. The only free parameters (to fit) are the carrier mobility in the perovskite and the trap density plus the charge capture coefficients. The maximum generation rate (G_{max}) is calculated by the transfer matrix model[52] and corresponds to a maximum short-circuit current density of 19.9 mA/cm^2. The charge carrier mobilities extracted from the fit are in agreement with reported values for $CH_3NH_3PbI_3$ solar cells.[11,23] Bimolecular recombination takes place in the perovskite bulk with the recombination coefficient 1×10^{-9} cm^3 s^{-1}.[11] Trap-assisted recombination takes place at material interfaces (HTL/perovskite and perovskite/ETL) and at GBs. Here, $C_p < C_n$ states that the probability per unit time of hole capture by a filled electron trap is lower than that of the electron capture by a filled hole trap. This is in agreement with the realization of long-lived holes[44] in PSCs.

Even in the presence of traps at GBs in the perovskite layer, trap-assisted recombination at interfaces is the dominant loss mechanism, in agreement with our previous report.[15] At solar fluences, traps at GBs are filled with photogenerated charges and become neutral and hence do not act as space charge. In addition, due to the low trap density at GBs and the existence of an alternate pathway (bimolecular) for charge carriers to recombine, GBs are benign at solar fluences.

As seen in Figure 4a, the n−i−p cell shows improved performance with the V_{OC} and FF reaching 1.12 V and 81%, respectively. From the fit parameters in Table 1, the trap density at the HTL/perovskite interface (which is the front interface for the p−i−n cell) is higher than that at the perovskite/ETL interface (which is the front interface for the n−i−p cell). Because the quality of the front interface has a greater impact on the device performance,[15] the n−i−p cell performs better. The enhanced performance of the n−i−p cell also derives from the higher conductivity of the doped ETL as compared to doped HTL, which boosts charge extraction at the front interface, and in part due to the use of gold (Au) as the anode, which eliminates the hole energetic offset that is otherwise present in the p−i−n cell where ITO is used as the anode.[9]

The light intensity dependence of the V_{OC} and FF for both p−i−n and n−i−p cells is shown in Figure 5a,b. The light intensity dependence of V_{OC} reveals the dominant mechanism in solar cells, with slopes of kT/q and $2kT/q$ indicating dominant bimolecular and trap-assisted recombination, respec-

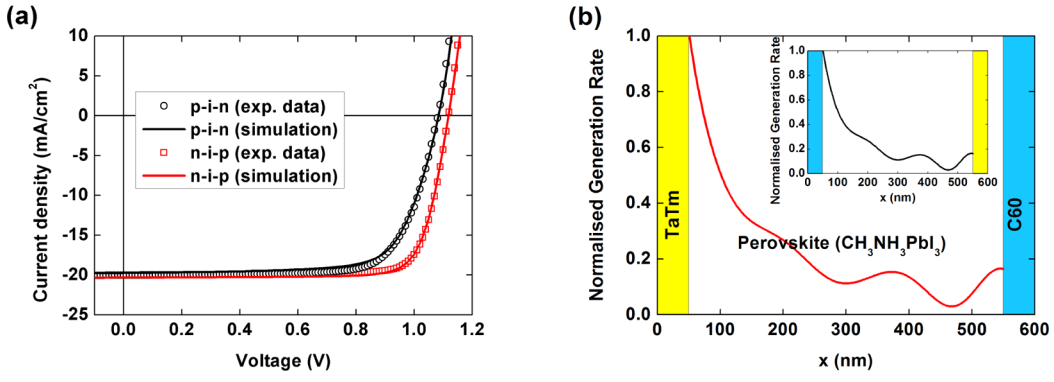

Figure 4. (a) *J*−*V* characteristics of p−i−n and n−i−p PSCs. The open symbols are experimental data for vacuum-deposited $CH_3NH_3PbI_3$ solar cells.[9] The solid lines represent the simulations. (b) Normalized generation profile for the p−i−n and n−i−p (inset) solar cell as calculated using the transfer matrix model.[52]

DOI: 10.1021/acsenergylett.7b00236
ACS Energy Lett. 2017, 2, 1214−1222

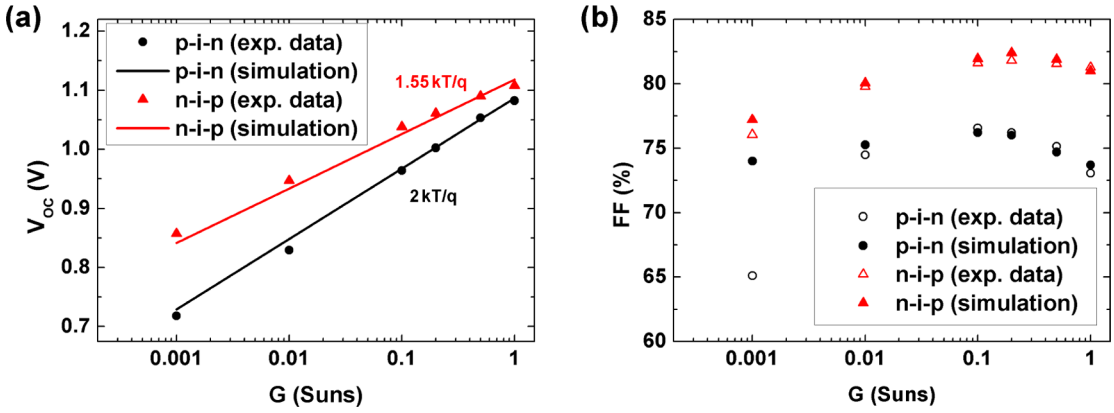

Figure 5. Light intensity dependence of (a) V_{OC} and (b) FF for both p−i−n and n−i−p cells. The filled symbols and lines in (a) represent experimental data and simulation, respectively. The open and filled symbols in (b) represent experimental data and simulation, respectively.

tively.[56,57] Due to the superior quality of the front interface in the n−i−p cell, trap-assisted recombination is suppressed (slope = $1.55kT/q$) as compared to the p−i−n cell (slope = $2.1kT/q$). Under open-circuit conditions, no current (hence no power) is extracted from the solar cell. As a solar cell is operated close to maximum power, the FF is the more relevant characteristic. The light intensity dependence of the FF trend reveals that there is some competition between bimolecular and trap-assisted recombination in these cells. In a pure bimolecular recombination scenario, FF increases with decreasing light intensity as the recombination rate is proportional to the product of charge carrier densities (which decreases with decreasing light intensity). For a pure trap-assisted recombination scenario, FF decreases with decreasing light intensity as the proportion of free charges recombining with trapped charges (the number of traps remains the same) increases with decreasing light intensity. Now, as can be seen in Figure 5b, bimolecular recombination dominates for light intensities above 0.1 Sun, while trap-assisted recombination does so below 0.1 Sun. The FF is more sensitive (as compared to V_{OC}) to leakage at lower light intensities[58] and hence the anomalous FF value of the p−i−n cell at 0.001 Sun.

Although traps at GBs and interfaces are likely to be charged (due to accumulated ionic defects) when empty and hence neutral when filled, the sign of the filled trap has little to do with the overall device performance when the solar cell in question is efficient, with fused GBs (low trap densities). The PSCs used here show compact morphology and have high efficiencies reaching 20% with little or no hysteresis,[9] and hence, the sign of the filled traps shows only a marginal change in device performance (Figure S2 in the SI). On the other hand, solar cells with open GBs (high trap densities) show high sensitivity to the sign of filled traps at GBs, as shown in Figure S2. Charged filled traps lead to faster SRH recombination due to the Coulombic attraction between opposite charged species (a negative filled trap and a hole). However, even then, some PSCs with open GBs (high trap densities) show decent efficiencies (~12%).[47] This can be attributed to the likely case of the existence of charged empty traps (accumulated V_I^+ at GBs and interfaces) and thus neutral filled traps, which lowers the SRH recombination rate in PSCs. Solar cell preparation methods are likely to influence the properties of traps, which is why there seems to be no agreement in the literature about the impact of GBs on the device performance.[19−21,23,24]

Until this point, we simulated the current−voltage (J−V) scans under "stabilized" conditions (an infinitely slow J−V scan), such that all mobile iodide ions (X_a) given by eq 10 (compensating the presence of accumulated iodide vacancies V_I^+ at GBs/interfaces acting as traps and recombination centers for photogenerated charge carriers) were allowed to redistribute at every step of the scan. This naturally resulted in hysteresis-free device characteristics as the forward and reverse scans yielded the same J−V curve. While the role of preconditioning and scan rate is more or less clear in the context of J−V hysteresis in $CH_3NH_3PbI_3$ solar cells,[59−63] we would like to answer the following question: Is there a relation between the density of trap states, the density of defect mobile ions, and the degree of hysteresis seen in PSCs?

The trap density in the p−i−n and n−i−p cells studied here is known from Table 1. In the model, the mobile iodide ion (X_a) density is assumed to be related to the trap density (accumulated V_I^+) by eq 10 because their origin is the same (dislocation of iodide ions). We now simulate the extreme case (where cells would show maximum hysteresis) of a fast voltage scan rate ($V_{scan} = \infty$) after preconditioning (infinitely long) at −0.2 V (for forward scan) and l.2 V (for reverse scan) bias. The fast forward scan simulation is performed after preconditioning the device at −0.2 V under illumination such that negative iodide ions are pushed toward the ETL and stay put throughout the scan. For the fast reverse scan, the device is preconditioned at 1.2 V under illumination such that the iodide ions are pushed away from the ETL and their distribution remains fixed during the scan. This gives us an envelope (two J−V curves enclosing a small area) that relates to the degree of hysteresis. The simulated hysteresis is shown in Figure 6 and is consistent with the experimentally observed little hysteresis in p−i−n cells and no hysteresis in n−i−p cells that we study here.[9] In these cells made by some of us, the degree of measured J−V hysteresis is relatively unchanged when the scans are performed with or without preconditioning, irrespective of the scan rate.[9] The simulation details of the fast scans and "stabilized" scans are included in the SI. It is clear that high-performing PSCs are likely to show little or no hysteresis because they contain a low density of traps and hence mobile defect ions. This is in agreement with Calado et al.,[64] who provide evidence that devices with minimal hysteresis still have moving ions but low trap densities that results in decreased recombination strength in the device and therefore little hysteresis. As shown in Figure S3, poor solar cells with high

DOI: 10.1021/acsenergylett.7b00236
ACS Energy Lett. 2017, 2, 1214−1222

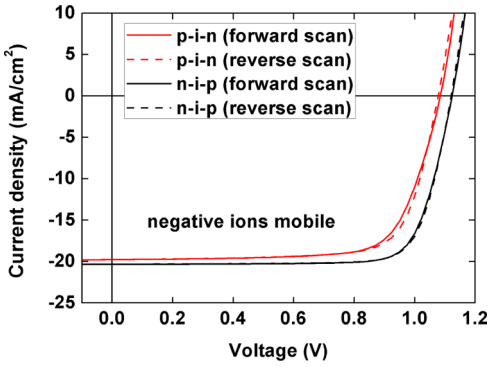

Figure 6. Simulated forward/reverse scan of p−i−n and n−i−p cells showing hysteresis in the $J-V$ curves when negative iodide ions ($X_a = 4 \times 10^{14}$ cm^{-3}) are mobile. The forward scan is performed after preconditioning at −0.2 V, and the reverse scan is carried out after preconditioning at 1.2 V.

trap density (and thus defect ions) show more hysteresis in the $J-V$ characteristics. Therefore, defect states or mobile ions not only limit the device performance but also play a role in the hysteresis observed in their $J-V$ characteristics of PSCs.

An estimate of the density of the mobile ions in the specific set of PSCs studied in this paper would be $X_a \approx 10^{15}$ cm^{-3} at the most.

It is possible that ionic defects other than the iodide complexes act as trap-assisted recombination centers and contribute to $J-V$ hysteresis. However, the activation energies for migration of I complexes are much lower as compared to those of other ionic (CH_3NH_3, Pb, etc.) complexes,[38,63] and hence, I complexes are more likely to influence the device optoelectronic performance.[45]

In conclusion, we investigated the attributes of the primary trap-assisted recombination channels (GBs and interfaces) and their correlation to defect ions in PSCs. We achieved this by using a device model[15] to fit the simulations to the experimental data of efficient p−i−n and n−i−p $CH_3NH_3PbI_3$ solar cells. The model utilized an extensive experimental data set (Table 1) as input, and the only free parameters (to fit) were the carrier mobility in the perovskite and the trap density plus the charge capture coefficients. Excellent agreement was found between the simulated data and experimental data, including the light intensity dependence of V_{OC} and FF. We found that despite the presence of traps at GBs, their neutral (when filled with photogenerated charges) disposition along with the long-lived nature of holes leads to the high performance of PSCs. The sign (if charged or neutral when filled) of traps is of little importance in efficient solar cells with compact morphologies (fused GBs, low trap density). On the other hand, solar cells with noncompact morphologies (open GBs, high trap density) are sensitive to the sign of the traps and hence cell preparation methods (e.g., under/overstoichiometric routes, environmental conditions). Even in the presence of traps at GBs in the perovskite layer, trap-assisted recombination at interfaces is the dominant loss mechanism, in agreement with our previous report.[15] We found a direct correlation between the density of trap states, the density of mobile ions, and the degree of hysteresis observed in the current−voltage ($J-V$) characteristics. High-performing PSCs are likely to show little or no hysteresis because they contain low density of traps and hence ions, while poor solar cells with high trap density (and thus ions) show more hysteresis. Therefore, defects states or mobile ions not only limit the device performance but also play a role in the hysteresis observed in the $J-V$ characteristics of PSCs. We found that the specific set of devices studied in this Letter contain a defect mobile ion density on the order 10^{15} cm^{-3} at the most.

Focus should be directed toward passivation of traps at interfaces (HTL/perovskite and perovskite/ETL) where trap-assisted recombination dominates, while the use of polycrystalline perovskite films with fused GBs as absorber is good enough to achieve high-performance solar cells.

■ ASSOCIATED CONTENT

Supporting Information

The Supporting Information is available free of charge on the ACS Publications website at DOI: 10.1021/acsenergylett.7b00236.

Simulation details, optical data, and additional results (PDF)

■ AUTHOR INFORMATION

Corresponding Author

*E-mail: l.j.a.koster@rug.nl.

ORCID

Henk J. Bolink: 0000-0001-9784-6253

L. Jan Anton Koster: 0000-0002-6558-5295

Notes

The authors declare no competing financial interest.

■ ACKNOWLEDGMENTS

The Valencian team acknowledges financial support from the Spanish Ministry of Economy and Competitiveness (MINECO) via the Unidad de Excelencia María de Maeztu MDM-2015-0538 and MAT2014-55200, PCIN-2015-255, and the Generalitat Valenciana (Prometeo/2016/135). C.M. and M.S. thank the MINECO for their pre- and postdoctoral (JdC) contracts. This work is part of the Industrial Partnership Programme (IPP) "Computational sciences for energy research" of the Foundation for Fundamental Research on Matter (FOM), which is part of The Netherlands Organisation for Scientific Research (NWO). This research programme is cofinanced by Shell Global Solutions International B.V. This is a publication by the FOM Focus Group "Next Generation Organic Photovoltaics", participating in the Dutch Institute for Fundamental Energy Research (DIFFER).

■ REFERENCES

(1) Green, M. A.; Emery, K.; Hishikawa, Y.; Warta, W.; Dunlop, E. D.; Levi, D. H.; Ho-Baillie, A. W. Solar cell efficiency tables (version 49). *Prog. Photovoltaics* **2017**, *25*, 3.

(2) Kojima, A.; Teshima, K.; Shirai, Y.; Miyasaka, T. Organometal halide perovskites as visible-light sensitizers for photovoltaic cells. *J. Am. Chem. Soc.* **2009**, *131*, 6050−6051.

(3) Stranks, S. D.; Eperon, G. E.; Grancini, G.; Menelaou, C.; Alcocer, M. J.; Leijtens, T.; Herz, L. M.; Petrozza, A.; Snaith, H. J. Electron-hole diffusion lengths exceeding 1 micrometer in an organometal trihalide perovskite absorber. *Science* **2013**, *342*, 341−344.

(4) Edri, E.; Kirmayer, S.; Mukhopadhyay, S.; Gartsman, K.; Hodes, G.; Cahen, D. Elucidating the charge carrier separation and working mechanism of CH3NH3PbI3-xClx perovskite solar cells. *Nat. Commun.* **2014**, *5*, 3461.

DOI: 10.1021/acsenergylett.7b00236
ACS Energy Lett. 2017, 2, 1214−1222

(5) Liu, M.; Johnston, M. B.; Snaith, H. J. Efficient planar heterojunction perovskite solar cells by vapour deposition. *Nature* **2013**, *501*, 395−398.
(6) Malinkiewicz, O.; Yella, A.; Lee, Y. H.; Espallargas, G. M.; Graetzel, M.; Nazeeruddin, M. K.; Bolink, H. J. Perovskite solar cells employing organic charge-transport layers. *Nat. Photonics* **2013**, *8*, 128−132.
(7) You, J.; et al. Low-temperature solution-processed perovskite solar cells with high efficiency and flexibility. *ACS Nano* **2014**, *8*, 1674−1680.
(8) Nie, W.; et al. High-efficiency solution-processed perovskite solar cells with millimeter-scale grains. *Science* **2015**, *347*, 522−525.
(9) Momblona, C.; Gil-Escrig, L.; Bandiello, E.; Hutter, E. M.; Sessolo, M.; Lederer, K.; Blochwitz-Nimoth, J.; Bolink, H. J. Efficient vacuum deposited pin and nip perovskite solar cells employing doped charge transport layers. *Energy Environ. Sci.* **2016**, *9*, 3456−3463.
(10) Sha, W. E. I.; Ren, X.; Chen, L.; Choy, W. C. The efficiency limit of CH3NH3PbI3 perovskite solar cells. *Appl. Phys. Lett.* **2015**, *106*, 221104.
(11) Wehrenfennig, C.; Eperon, G. E.; Johnston, M. B.; Snaith, H. J.; Herz, L. M. High charge carrier mobilities and lifetimes in organolead trihalide perovskites. *Adv. Mater.* **2014**, *26*, 1584−1589.
(12) Wetzelaer, G. A. H.; Scheepers, M.; Sempere, A. M.; Momblona, C.; Ávila, J.; Bolink, H. J. Trap-Assisted Non-Radiative Recombination in Organic-Inorganic Perovskite Solar Cells. *Adv. Mater.* **2015**, *27*, 1837−1841.
(13) Johnston, M. B.; Herz, L. M. Hybrid perovskites for photovoltaics: Charge-carrier recombination, diffusion, and radiative efficiencies. *Acc. Chem. Res.* **2016**, *49*, 146−154.
(14) Tress, W.; Marinova, N.; Inganäs, O.; Nazeeruddin, M.; Zakeeruddin, S. M.; Graetzel, M. Predicting the Open-Circuit Voltage of CH3NH3PbI3 Perovskite Solar Cells Using Electroluminescence and Photovoltaic Quantum Efficiency Spectra: the Role of Radiative and Non-Radiative Recombination. *Adv. Energy Mater.* **2015**, *5*, 1400812.
(15) Sherkar, T. S.; Momblona, C.; Gil-Escrig, L.; Bolink, H. J.; Koster, L. J. A. Improving the Performance of Perovskite Solar Cells: Insights From a Validated Device Model. *Adv. Energy Mater.* **2017**, 1602432.
(16) Shao, Y.; et al. Grain boundary dominated ion migration in polycrystalline organic-inorganic halide perovskite films. *Energy Environ. Sci.* **2016**, *9*, 1752−1759.
(17) Cui, P.; Fu, P.; Wei, D.; Li, M.; Song, D.; Yue, X.; Li, Y.; Zhang, Z.; Li, Y.; Mbengue, J. M. Reduced surface defects of organometallic perovskite by thermal annealing for highly efficient perovskite solar cells. *RSC Adv.* **2015**, *5*, 75622−75629.
(18) Wu, X.; Trinh, M. T.; Niesner, D.; Zhu, H.; Norman, Z.; Owen, J. S.; Yaffe, O.; Kudisch, B. J.; Zhu, X.-Y. Trap states in lead iodide perovskites. *J. Am. Chem. Soc.* **2015**, *137*, 2089−2096.
(19) Chen, Q.; Zhou, H.; Song, T.-B.; Luo, S.; Hong, Z.; Duan, H.-S.; Dou, L.; Liu, Y.; Yang, Y. Controllable self-induced passivation of hybrid lead iodide perovskites toward high performance solar cells. *Nano Lett.* **2014**, *14*, 4158−4163.
(20) MacDonald, G. A.; Yang, M.; Berweger, S.; Killgore, J. P.; Kabos, P.; Berry, J. J.; Zhu, K.; DelRio, F. W. Methylammonium lead iodide grain boundaries exhibit depth-dependent electrical properties. *Energy Environ. Sci.* **2016**, *9*, 3642−3649.
(21) Yun, J. S.; Ho-Baillie, A.; Huang, S.; Woo, S. H.; Heo, Y.; Seidel, J.; Huang, F.; Cheng, Y.-B.; Green, M. A. Benefit of grain boundaries in organic-inorganic halide planar perovskite solar cells. *J. Phys. Chem. Lett.* **2015**, *6*, 875−880.
(22) Jacobsson, T. J.; et al. Unreacted PbI2 as a Double-Edged Sword for Enhancing the Performance of Perovskite Solar Cells. *J. Am. Chem. Soc.* **2016**, *138*, 10331−10343.
(23) de Quilettes, D. W.; Vorpahl, S. M.; Stranks, S. D.; Nagaoka, H.; Eperon, G. E.; Ziffer, M. E.; Snaith, H. J.; Ginger, D. S. Impact of microstructure on local carrier lifetime in perovskite solar cells. *Science* **2015**, *348*, 683−686.
(24) Bischak, C. G.; Sanehira, E. M.; Precht, J. T.; Luther, J. M.; Ginsberg, N. S. Heterogeneous Charge Carrier Dynamics in Organic-Inorganic Hybrid Materials: Nanoscale Lateral and Depth-Dependent Variation of Recombination Rates in Methylammonium Lead Halide Perovskite Thin Films. *Nano Lett.* **2015**, *15*, 4799−4807.
(25) Ono, L. K.; Qi, Y. Surface and Interface Aspects of Organometal Halide Perovskite Materials and Solar Cells. *J. Phys. Chem. Lett.* **2016**, *7*, 4764−4794.
(26) Nelson, J. *The Physics of Solar Cells*; Imperial College Press: London, 2003.
(27) Visoly-Fisher, I.; Cohen, S. R.; Gartsman, K.; Ruzin, A.; Cahen, D. Understanding the Beneficial Role of Grain Boundaries in Polycrystalline Solar Cells from Single-Grain-Boundary Scanning Probe Microscopy. *Adv. Funct. Mater.* **2006**, *16*, 649−660.
(28) Li, C.; et al. Grain-boundary-enhanced carrier collection in CdTe solar cells. *Phys. Rev. Lett.* **2014**, *112*, 156103.
(29) Distefano, T.; Cuomo, J. Reduction of grain boundary recombination in polycrystalline silicon solar cells. *Appl. Phys. Lett.* **1977**, *30*, 351−353.
(30) Gloeckler, M.; Sites, J. R.; Metzger, W. K. Grain-boundary recombination in Cu (In, Ga) Se2 solar cells. *J. Appl. Phys.* **2005**, *98*, 113704.
(31) Seto, J. Y. The electrical properties of polycrystalline silicon films. *J. Appl. Phys.* **1975**, *46*, 5247−5254.
(32) Landsberg, P.; Abrahams, M. Effects of surface states and of excitation on barrier heights in a simple model of a grain boundary or a surface. *J. Appl. Phys.* **1984**, *55*, 4284−4293.
(33) Card, H. C.; Yang, E. S. Electronic processes at grain boundaries in polycrystalline semiconductors under optical illumination. *IEEE Trans. Electron Devices* **1977**, *24*, 397−402.
(34) Yin, W.-J.; Yang, J.-H.; Kang, J.; Yan, Y.; Wei, S.-H. Halide perovskite materials for solar cells: a theoretical review. *J. Mater. Chem. A* **2015**, *3*, 8926−8942.
(35) Walsh, A.; Scanlon, D. O.; Chen, S.; Gong, X.; Wei, S.-H. Self-Regulation Mechanism for Charged Point Defects in Hybrid Halide Perovskites. *Angew. Chem.* **2015**, *127*, 1811−1814.
(36) Yin, W.-J.; Shi, T.; Yan, Y. Unusual defect physics in CH3NH3PbI3 perovskite solar cell absorber. *Appl. Phys. Lett.* **2014**, *104*, 063903.
(37) Selberherr, S. *Analysis and Simulation of Semiconductor Devices*; Springer-Verlag: Vienna, 1984.
(38) Eames, C.; Frost, J. M.; Barnes, P. R.; O'regan, B. C.; Walsh, A.; Islam, M. S. Ionic transport in hybrid lead iodide perovskite solar cells. *Nat. Commun.* **2015**, *6*, 7497.
(39) Azpiroz, J. M.; Mosconi, E.; Bisquert, J.; de Angelis, F. Defect migration in methylammonium lead iodide and its role in perovskite solar cell operation. *Energy Environ. Sci.* **2015**, *8*, 2118−2127.
(40) Yuan, Y.; Huang, J. Ion Migration in Organometal Trihalide Perovskite and Its Impact on Photovoltaic Efficiency and Stability. *Acc. Chem. Res.* **2016**, *49*, 286−293.
(41) Simmons, J.; Taylor, G. Nonequilibrium steady-state statistics and associated effects for insulators and semiconductors containing an arbitrary distribution of traps. *Phys. Rev. B* **1971**, *4*, 502.
(42) Koster, L. J. A.; Smits, E. C. P.; Mihailetchi, V. D.; Blom, P. W. M. Device model for the operation of polymer/fullerene bulk heterojunction solar cells. *Phys. Rev. B: Condens. Matter Mater. Phys.* **2005**, *72*, 085205.
(43) Leijtens, T.; Stranks, S. D.; Eperon, G. E.; Lindblad, R.; Johansson, E. M.; McPherson, I. J.; Rensmo, H.; Ball, J. M.; Lee, M. M.; Snaith, H. J. Electronic properties of meso-superstructured and planar organometal halide perovskite films: charge trapping, photodoping, and carrier mobility. *ACS Nano* **2014**, *8*, 7147−7155.
(44) Leijtens, T.; Eperon, G. E.; Barker, A. J.; Grancini, G.; Zhang, W.; Ball, J. M.; Kandada, A. R. S.; Snaith, H. J.; Petrozza, A. Carrier trapping and recombination: the role of defect physics in enhancing the open circuit voltage of metal halide perovskite solar cells. *Energy Environ. Sci.* **2016**, *9*, 3472−3481.
(45) deQuilettes, D. W.; Zhang, W.; Burlakov, V. M.; Graham, D. J.; Leijtens, T.; Osherov, A.; Bulović, V.; Snaith, H. J.; Ginger, D. S.;

DOI: 10.1021/acsenergylett.7b00236
ACS Energy Lett. 2017, 2, 1214−1222

Stranks, S. D. Photo-induced halide redistribution in organic-inorganic perovskite films. *Nat. Commun.* **2016**, *7*, 11683.
(46) Du, M.-H. Density functional calculations of native defects in CH3NH3PbI3: effects of spin-orbit coupling and self-interaction error. *J. Phys. Chem. Lett.* **2015**, *6*, 1461−1466.
(47) Shao, S.; Abdu-Aguye, M.; Sherkar, T. S.; Fang, H.-H.; Adjokatse, S.; Brink, G. t.; Kooi, B. J.; Koster, L.; Loi, M. A. The Effect of the Microstructure on Trap-Assisted Recombination and Light Soaking Phenomenon in Hybrid Perovskite Solar Cells. *Adv. Funct. Mater.* **2016**, *26*, 8094−8102.
(48) Uratani, H.; Yamashita, K. Charge Carrier Trapping at Surface Defects of Perovskite Solar Cell Absorbers: A First-Principles Study. *J. Phys. Chem. Lett.* **2017**, *8*, 742−746.
(49) Sherkar, T. S.; Koster, L. J. A. Can ferroelectric polarization explain the high performance of hybrid halide perovskite solar cells? *Phys. Chem. Chem. Phys.* **2016**, *18*, 331−338.
(50) Yuan, Y.; Li, T.; Wang, Q.; Xing, J.; Gruverman, A.; Huang, J. Anomalous photovoltaic effect in organic-inorganic hybrid perovskite solar cells. *Science Adv.* **2017**, *3*, e1602164.
(51) Xing, G.; Mathews, N.; Sun, S.; Lim, S. S.; Lam, Y. M.; Grätzel, M.; Mhaisalkar, S.; Sum, T. C. Long-range balanced electron-and hole-transport lengths in organic-inorganic CH3NH3PbI3. *Science* **2013**, *342*, 344−347.
(52) Burkhard, G. F.; Hoke, E. T.; McGehee, M. D. Accounting for interference, scattering, and electrode absorption to make accurate internal quantum efficiency measurements in organic and other thin solar cells. *Adv. Mater.* **2010**, *22*, 3293−3297.
(53) Tress, W. Device Physics of Organic Solar Cells. Ph.D. thesis, TU Dresden, Dresden, Germany, 2011.
(54) Brivio, F.; Butler, K. T.; Walsh, A.; van Schilfgaarde, M. Relativistic quasiparticle self-consistent electronic structure of hybrid halide perovskite photovoltaic absorbers. *Phys. Rev. B: Condens. Matter Mater. Phys.* **2014**, *89*, 155204.
(55) Mönch, T.; Sherkar, T. S.; Koster, L. J. A.; Friederich, P.; Riede, M.; Formanek, P.; Koerner, C.; Vandewal, K.; Wenzel, W.; Leo, K. Experimental and theoretical study of phase separation in ZnPc: C 60 blends. *Org. Electron.* **2015**, *27*, 183−191.
(56) Koster, L. J. A.; Mihailetchi, V. D.; Ramaker, R.; Blom, P. W. Light intensity dependence of open-circuit voltage of polymer: fullerene solar cells. *Appl. Phys. Lett.* **2005**, *86*, 123509−123509.
(57) Mandoc, M.; Kooistra, F.; Hummelen, J.; De Boer, B.; Blom, P. Effect of traps on the performance of bulk heterojunction organic solar cells. *Appl. Phys. Lett.* **2007**, *91*, 263505.
(58) Tvingstedt, K.; Gil-Escrig, L.; Momblona, C.; Rieder, P.; Kiermasch, D.; Sessolo, M.; Baumann, A.; Bolink, H. J.; Dyakonov, V. Removing Leakage and Surface Recombination in Planar Perovskite Solar Cells. *ACS Energy Letters* **2017**, *2*, 424−430.
(59) Snaith, H. J.; Abate, A.; Ball, J. M.; Eperon, G. E.; Leijtens, T.; Noel, N. K.; Stranks, S. D.; Wang, J. T.-W.; Wojciechowski, K.; Zhang, W. Anomalous hysteresis in perovskite solar cells. *J. Phys. Chem. Lett.* **2014**, *5*, 1511−1515.
(60) Tress, W.; Marinova, N.; Moehl, T.; Zakeeruddin, S. M.; Nazeeruddin, M. K.; Grätzel, M. Understanding the rate-dependent J−V hysteresis, slow time component, and aging in CH 3 NH 3 PbI 3 perovskite solar cells: the role of a compensated electric field. *Energy Environ. Sci.* **2015**, *8*, 995−1004.
(61) Unger, E. L.; Hoke, E. T.; Bailie, C. D.; Nguyen, W. H.; Bowring, A. R.; Heumüller, T.; Christoforo, M. G.; McGehee, M. D. Hysteresis and transient behavior in current-voltage measurements of hybrid-perovskite absorber solar cells. *Energy Environ. Sci.* **2014**, *7*, 3690−3698.
(62) Richardson, G.; O'Kane, S. E.; Niemann, R. G.; Peltola, T. A.; Foster, J. M.; Cameron, P. J.; Walker, A. B. Can slow-moving ions explain hysteresis in the current−voltage curves of perovskite solar cells? *Energy Environ. Sci.* **2016**, *9*, 1476−1485.
(63) Meloni, S.; et al. Ionic polarization-induced current-voltage hysteresis in CH3NH3PbX3 perovskite solar cells. *Nat. Commun.* **2016**, *7*, 10334.
(64) Calado, P.; Telford, A. M.; Bryant, D.; Li, X.; Nelson, J.; O'regan, B. C.; Barnes, P. R. Evidence for ion migration in hybrid perovskite solar cells with minimal hysteresis. *Nat. Commun.* **2016**, *7*, 13831.

DOI: 10.1021/acsenergylett.7b00236
ACS Energy Lett. 2017, 2, 1214−1222